Three-dimensionalization of the stratified mixing layer at high Reynolds number

A. Mashayek and W. R. Peltier

Citation: Physics of Fluids **23**, 111701 (2011); doi: 10.1063/1.3651269
View online: http://dx.doi.org/10.1063/1.3651269
View Table of Contents: http://scitation.aip.org/content/aip/journal/pof2/23/11?ver=pdfcov
Published by the AIP Publishing

Three-dimensionalization of the stratified mixing layer at high Reynolds number

A. Mashayek and W. R. Peltier
Physics Department, University of Toronto, Toronto, Ontario M5S 1A7, Canada

(Received 10 May 2011; accepted 19 August 2011; published online 17 November 2011)

Numerical analyses of the stability of a stratified two-dimensional Kelvin-Helmholtz billow against three dimensional disturbances provide a theoretical means of identifying the primary mechanism(s) that induce transition to turbulence. We identify, through fully resolved three-dimensional numerical simulations, secondary modes of instability which have been suggested by recent observations to be responsible for this transition. Our analyses lead us to two primary conclusions. First, as the Reynolds number is increased at a fixed stratification level, the vortex pairing process may be entirely suppressed by the rapid growth of three-dimensional secondary instabilities. Second, the new transition mechanisms identified herein have significant implications for the efficiency of mixing in the turbulent flow that develops subsequent to saturation of the secondary instabilities. © *2011 American Institute of Physics*. [doi:10.1063/1.3651269]

Stratified free shear flows are known to be susceptible to primary instabilities which are most often inherently two-dimensional (2D). One of the most commonly observed of these instabilities is the Kelvin-Helmholtz (KH) instability. The primary KH waves are susceptible to 3D secondary instabilities which facilitate a rapid transition to turbulence. Among such secondary instabilities are the pairing instability,[1] the shear aligned convective instability (SCI) which occurs in the statically unstable regions inside the vortex cores of the train of KH billows,[2] the secondary shear instability (SSI) of the vorticity layer (braid) connecting the vortex cores in the train of KH billows,[3–5] and the stagnation point instability (SPI) which is a phase-locked instability local to the braid stagnation point.[1,6] Although formation of KH billows at high Reynolds numbers have long been observed in the atmosphere and in the oceanic thermocline,[7] recent observations have revealed trains of KH billows forming in the deep ocean[8] and in estuarine shear zones.[9] These studies have reported the observation of enhanced mixing in the braid of the KH billows due to secondary instabilities which seem to be of shear type, therefore suggesting that the SCI of Klaassen and Peltier (1985) might not be the sole mechanism responsible for turbulent collapse. Our recent theoretical analyses[6] have revealed secondary instabilities localized to the braid in addition to the convective instability inside the cores. It is our goal in this work to investigate the emergence of different secondary instabilities, their interactions, and their implications for irreversible turbulent mixing.

We consider evolution of a stratified shear layer with initial background profiles of $\bar{U}(z) = U_0 \tanh(z/h)$ and $\bar{\rho}(z) = \rho_a - \rho_0 \tanh(Rz/h)$, where U_0 and ρ_0 are reference velocity and density, and where h is half the shear layer thickness, which is chosen to be 1.1 based on laboratory experimental observations in which the working fluid is salt stratified water.

We also consider the equations of motion, incompressibility, and continuity in dimensionless form similar to Caulfield and Peltier[10] (hereafter referred to as *CP00*). The Reynolds number is defined by $Re = U_0 h/\nu$ where ν is the kinematic viscosity and the Prandtl number by $Pr = \nu/\kappa$ where κ is the thermal diffusivity. The stratification at the center of the shear layer is measured by Ri_0, the value of the gradient Richardson number $Ri(z) = N^2/(d\bar{U}/dz)^2$ (where N is the buoyancy frequency) at the center line.

Direct numerical simulations (DNS) of the governing equations are employed to ensure that all relevant scales of motion are resolved. The pseudo-spectral algorithm we employ is that described in detail in Taylor.[11] Periodic boundary conditions are applied in the streamwise and cross-streamwise directions, while second-order energy-conserving finite differences are used in the vertical direction. Discrete conservation of mass, momentum, and energy are ensured by the numerical scheme. In the streamwise direction, the length of the numerical domain is set equal to two wavelengths of the most unstable mode of linear inviscid theory (i.e., 2×14.27) to allow the pairing instability to grow. The vertical extent of the computational domain is chosen to be sufficiently large to ensure that the flow remains unaffected by the horizontal boundaries (it is set to $30h$ where h is half the shear layer depth).

The flow field is initialized by the addition of a small perturbation in the form of the most unstable KH mode to the background velocity and density fields. To ensure that the initialization does not have any significant impact on the results, the kinetic energy associated with the initial disturbance is chosen to be only 10^{-5} times that of the background shear flow and limited to a vertical range of $5h$ from the center of the shear layer. To allow for an unbiased initiation of any secondary instability, small amplitude white noise is added to the velocity and density fields. Boundary conditions are free-slip impermeable on velocity components and zero density flux at the horizontal boundaries of the domain. Resolution studies and flow diagnostic tools were employed to ensure the validity and accuracy of each simulation. In particular, it was ensured that the evolution equations for the total kinetic energy and the inherently three-dimensional perturbation kinetic energy (Eqs. 2.20 and 2.23 from *CP00*) were satisfied for all simulations. Specific information regarding the 3D numerical simulations discussed in this paper is provided in Table I. For the $Re < 4000$ cases, the experiments were repeated (but are not

TABLE I. Details of the numerical simulations.

Re	Ri_0	Pr	L_x	L_y	L_z	N_x	N_y	N_z
750	0.05	1	28.56	4	30	320	64	600
750	0.085	1	28.56	4	30	320	64	600
750	0.12	1	28.56	4	30	512	96	800
1000	0.12	1	28.54	3	30	768	96	800
4000	0.12	1	28.54	3	30	1024	128	1216
6000	0.12	1	28.54	3	30	1024	128	1216
8000	0.12	1	28.54	3	30	1024	128	1216

discussed herein) with twice and triple the spanwise extents (with the resolution also increased accordingly) to ensure that the fastest growing modes of the secondary instabilities (which will be discussed in the following paragraph) are resolved.

Figure 1 shows the results of our 3D DNS calculations for Reynolds numbers of 750 and 1000 and for various Richardson numbers. For small to intermediate values of Ri_0, the pairing instability is the first mode to emerge followed by formation of convective rolls in the unstable regions inside the cores. For $Re = 750$, $Ri_0 = 0.085$, these vortices grow considerably during the development of the pairing process and lead to three-dimensionalization of the flow and transition to turbulence. The large scale structure of the flow, however, follows that imposed by the pairing process. For $Ri_0 = 0.12$, the SCI grows to high amplitude early in the flow evolution. The interaction between shear-aligned vortex rolls breaks the flow down to turbulence, but a moderate form of pairing still ensues in the turbulent phase. These simulations are different from those of *CP00* in that they allow for the pairing process (by including two wavelengths of the primary KH wave in the flow domain). In agreement with several experimental studies, our results show that vortex pairing is delayed with an increase in stratification. However, our results also show that this delay allows for large amplitude growth of 3D instabilities which break the flow down to turbulence, diminishing or (as will be shown for higher Re) suppressing the pairing process entirely. The same is true for a slightly higher $Re = 1000$ (at $Ri_0 = 0.12$), where emergence of SCI rolls leads to a rapid transition prior to the onset of pairing. At $Re = 1000$, there still exists a tendency for an upscale energy transfer, and pairing occurs in the turbulent phase of the flow as shown in the last panel of Figure 1. This turbulent-pairing induces far less vertical displacement in the shear layer (compared to the pre-turbulent pairing), and it has a much smaller influence on the energy exchange between the KH wave and the background flow and on irreversible mixing as will be shown. Analysis of a flow with $Re = 2000$, $Ri_0 = 0.12$ revealed similarity to the $Re = 1000$ case and hence is not presented.

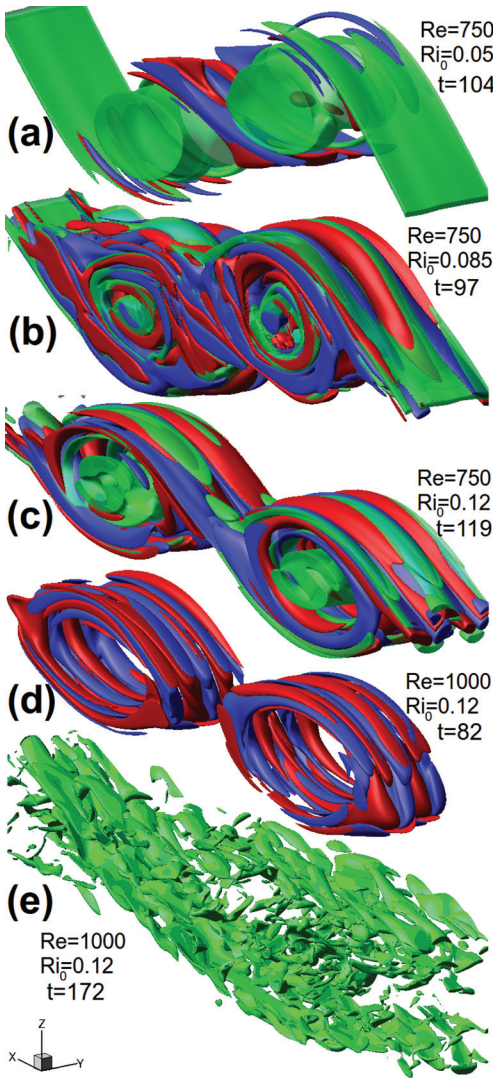

FIG. 1. (Color) Spanwise vorticity isosurface of $\omega_z = 0.72$ in green and streamwise vorticity isosurfaces of $\omega_x = 0.2$ (red) and $\omega_x = -0.2$ (blue).

Once the Reynolds number is sufficiently high, the transition to turbulence occurs through a series of different processes. As shown in the streamwise vorticity plot for $Re = 4000$ in Figures 2(a) and 2(b), the first secondary mode of instability to grow is the SPI. The growth of this mode, which extracts almost all of its energy from the stain field as discussed in *MP1*, gives rise to a phase-locked vortex at the braid stagnation point. Figure 2(a) shows that it is both the SPI and SCI and their interaction with one another which introduces three-dimensionality into the flow, leading to a rapid turbulent collapse with no trace of a vortex pairing mediated upscale cascade in the preturbulent or early stages of the turbulent phase.

As we increase the Reynolds number further, shear-induced vortices form on the braid in agreement with theoretical predictions[3,4,6] and observations.[9] Figure 2 includes plots of spanwise and streamwise vorticity isosurfaces for $Re = 8000$. As expected, SSI evolves at early stages of flow evolution (panel (c)). However, the SPI and SCI still emerge, grow rapidly, and lead to rapid breakup of the flow into turbulence which initiates at the corners of the cores (due to influence of SPI on the cores) as shown in frames (d) of the figure. A simulation was also performed for $Re = 6000$, and the resulting flow (not shown here) bore qualitative similarities to both of the $Re = 4000$ and $Re = 8000$ cases. The transport of the vortices formed on the braid to the periphery of the cores by the braid velocity field plays an important role in enhancing turbulent mixing inside the vortex cores.

As discussed in *MP1*, SSI and SPI are of different origins (the former is shear-driven and the latter strain-driven). A means of distinguishing between the two modes is to note that SPI is phase-locked, while SSI vortices are advected by the braid velocity. Moreover, stability analyses of *MP1*

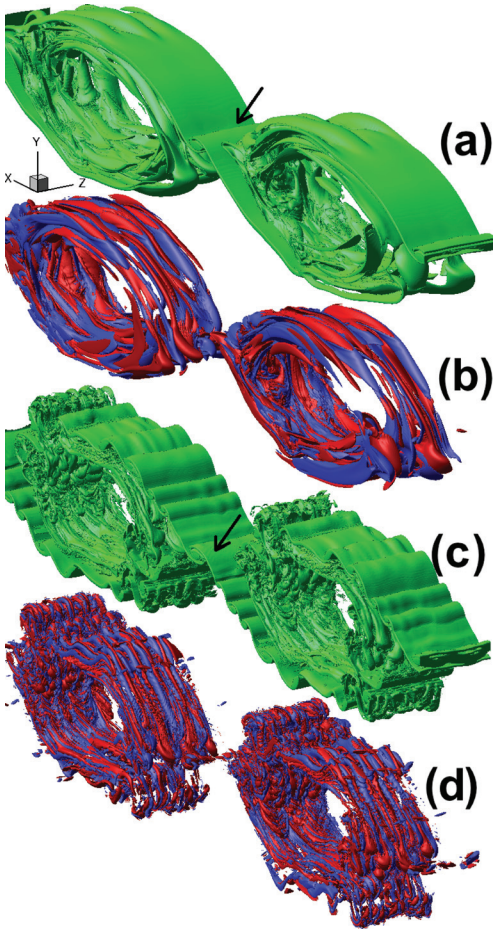

FIG. 2. (Color) Same as Figure 1. (a, b) for $Re = 4000$, $Ri_0 = 0.12$ at $t = 73$; (c) for $Re = 8000$, $Ri_0 = 0.12$ at $t = 67$. Arrows point to the phased-locked SPI on the braid.

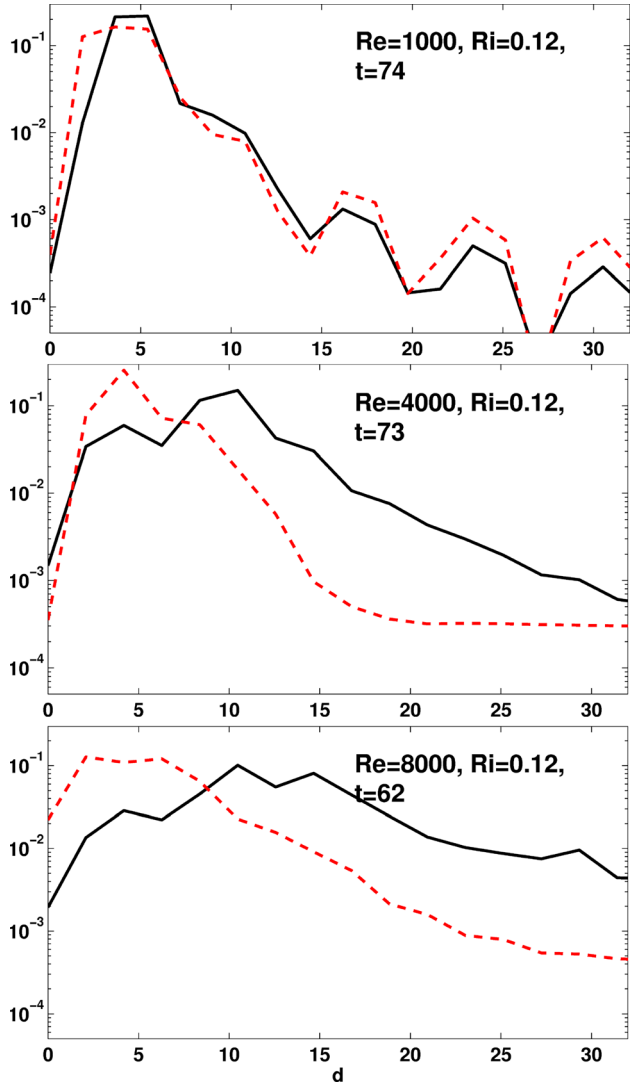

FIG. 3. (Color online) Variation of spanwise power spectrum density $P(d)$ (as defined in Eq. (6.5) of *CP00*) with the spanwise wavenumber d. Solid and dashed lines correspond to Fourier decomposition (with resolution of 128) of the core and the braid regions, respectively.

revealed that SPI is a highly 3D mode, whereas SSI is primarily a 2D mode (which can also be of small spanwise wavenumbers). To investigate predictions of *MP1*, we have used fast Fourier transformation to obtain a discretized spectral representation of the streamwise vorticity (following closely analyses of *CP00*). The decomposition is performed at a time within the short period of rapid saturation of 3D instabilities (similar to cases considered in *CP00*) and is focused on two regions of the flow field: the vortex core and the braid. The results are shown in Figure 3. For $Re = 1000$ and $Ri_0 = 0.12$, the power spectrum peaks at a spanwise wavenumber of ~ 6 which is in excellent agreement with theoretical prediction of *MP1*. The braid region is also dominated by the same wavenumber due to extension of SCI induced vortices to the braid (as shown in Figure 1(d)). For $Re = 4000$ and $Ri_0 = 0.12$, the core is dominated by SCI as shown in Figure 2(b). The braid region, however, hosts a phase-locked SPI vortex formed at the stagnation point (Figure 2(a)) which according to the clear peak of the braid power spectrum has a spanwise wavenumber of ~ 4. For $Re = 8000$ and $Ri_0 = 0.12$, the core remains dominated by SCI as shown in Figure 2(d). The braid region, however, hosts both the SPI and the shear driven SSI vortices as shown in Figure 2(c). The corresponding power spectrum shows that the long wave scales ($d \to 0$) are energized which is due to formation of 2D SSI vortices. The SPI also evolves for this case as shown by the arrow in Figure 2(c) and it has a wavelength of 7. Comparison between the power spectrum of the core and braid regions for the three cases in Figure 3 illustrates two points which are both in agreement with findings of *MP1*: (*i*) the scales of SCI and SPI decrease with Re and at sufficiently high Re, both modes become capable of injecting energy into a range of small scales; (*ii*) long wavelengths (small d) only become energized once 2D SSI vortices form on the braid.

To consider the influence of the secondary instability mechanisms responsible for transition to turbulence on the efficiency of irreversible mixing in free shear layers, we closely follow the analysis of *CP00* (Ref. 10). We define the irreversible mixing rate $\mathcal{M}$ as

$$\mathcal{M} = \frac{d\mathcal{P}_B}{dt} - \mathcal{D}_p, \tag{1}$$

where $\mathcal{P}_B$ is the background potential energy and $\mathcal{D}_p$ is the rate at which the potential energy of a statically stable density distribution would increase in the absence of macroscopic fluid motion through conversion of internal energy

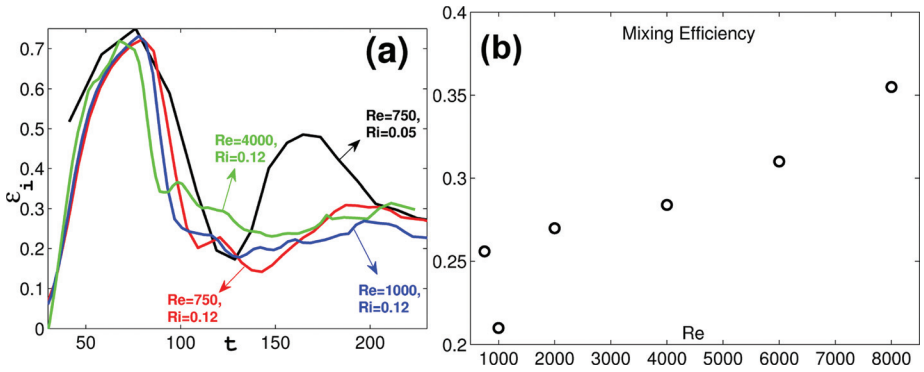

FIG. 4. (Color) (a) Instantaneous mixing efficiency, $\mathcal{E}_i$ and (b) post-transition cumulative mixing efficiency, $\mathcal{E}_{pc}$ as function of Re for cases with $Ri_0 = 0.12$. The dashed curve is a spline fit to the actual data points.

into potential energy. $\mathcal{P}_B$ is the minimum potential energy that the flow can attain; it is the potential energy of the flow if it were allowed to come to rest adiabatically. This energy is inaccessible to stirring and any increase in it is due to irreversible mixing (as expressed by Eq. (1)).[10,12,13]

Once $\mathcal{M}$ is calculated from Eq. (1), an instantaneous mixing efficiency can be defined as the ratio of kinetic energy lost by the fluid due to mixing to losses of kinetic energy owing to both irreversible mixing and viscous dissipation,

$$\mathcal{E}_i = \frac{\mathcal{M}}{\mathcal{M} + \epsilon}, \tag{2}$$

where ϵ the viscous dissipation.

Figure 4(a) shows the time evolution of $\mathcal{E}_i$ for several of the cases discussed. For all cases, the first peak represents laminar rolling up of the vorticity cores. During this preturbulent phase of flow evolution, instantaneous mixing is very large because of low viscous dissipation. After the transition to turbulence, $\mathcal{E}_i$ decreases substantially due to enhanced dissipation. The second peak in the curve for $Re = 750$, $Ri_0 = 0.05$ corresponds to vortex pairing (as shown in Figure 1(a)) which increases the efficiency by slightly suppressing 3D perturbations and thereby decreasing dissipation. The secondary peak for the $Re = 750$, $Ri_0 = 0.12$ case is less apparent compared to $Re = 750$, $Ri_0 = 0.05$ because of the rapid growth of 3D instabilities due to delay of the pairing process at higher stratification. For higher Reynolds number cases, 3D instabilities emerge earlier in flow evolution and break the flow down to turbulence rapidly and efficiently and suppress the pairing process. Curves for $Re = 1000$ and 4000 in Figure 4(a) show that the upscale cascade in the turbulent phase has very minor influence on the efficiency of mixing.

To enable direct comparison of the mixing efficiency with observational data, we also define a post-transition cumulative mixing efficiency, $\mathcal{E}_{pc}$, to account for mixing during the turbulent phase of the flow,

$$\mathcal{E}_{pc} = \frac{\int_{t^*}^{t} \mathcal{M}(t')\mathrm{d}t'}{\int_{t^*}^{t} \mathcal{M}(t')\mathrm{d}t' + \int_{t^*}^{t} \epsilon(t')\mathrm{d}t'}, \tag{3}$$

where t^* is the time of onset of turbulent motion (defined as the time during flow evolution when the 3D perturbations saturate[10]). Panel (b) of Figure 4 illustrates the variation in $\mathcal{E}_{pc}$ as a function of Re for the numerical experiments with $Ri_0 = 0.12$. At low Reynolds numbers (below 200), mixing becomes less efficient with increase in Re. This is because emergence of 3D secondary instabilities along with faster growth rates of the newly emerging (SPI and SSI) and previously existing (SCI) secondary modes significantly contribute to a rapid transition to turbulence prior to onset of vortex pairing (which enhances the efficiency of mixing greatly). For $Re > 2000$, pairing is suppressed and the efficiency of mixing increases with Re due to decrease in the length scales of 3D secondary instabilities and the length scales of the subsequent turbulent flow. We can expect the increase in $\mathcal{E}$ with Re to saturate at some value of Re higher than the maximum value considered here (8000).

Figure 4(b) implies that the value of 0.2, which is widely used as the efficiency of diapycnal mixing in free shear layers, needs to be reconsidered.[14–16] Variations in the mixing efficiency with changes in stratification level have already been well studied at low Reynolds number and has been reported in the observations.[15]

[1]G. P. Klaassen and W. R. Peltier, "The role of transverse secondary instabilities in the evolution of free shear layers," J. Fluid Mech. **202**, 367 (1989).
[2]G. P. Klaassen and W. R. Peltier, "The onset of turbulence in finite amplitude Kelvin-Helmholtz billows," J. Fluid Mech. **155**, 1 (1985).
[3]G. Corcos and F. Sherman, "Vorticity concentration and the dynamics of unstable free shear layers," J. Fluid Mech. **73**, 241 (1976).
[4]W. D. Smyth, "Secondary Kelvin-Helmholtz instability in weakly stratified shear flow," J. Fluid Mech. **497**, 67 (2003).
[5]C. Staquet, "Two-dimensional secondary instabilities in a strongly stratified shear layer," J. Fluid Mech. **296**, 73 (1995).
[6]A. Mashayek and W. R. Peltier, "The 'zoo' of secondary instabilities precursory to stratified shear flow transition. Part I: Shear aligned convection, pairing, and braid instabilities," J. Fluid Mech. (to be published).
[7]S. A. Thorpe, *The Turbulent Ocean* (Cambridge University, New York, 2005).
[8]H. Van Haren and L. Gostiaux, "A deep-ocean Kelvin-Helmholtz billow train," Geophys. Res. lett. **37**, L03605, doi:10.1029/2009GL041890 (2010).
[9]W. R. Geyer, A. C. Lavery, M. E. Scully, and J. H. Trowbridge, "Mixing by shear instability at high Reynolds number," Geophys. Res. Lett. **37**, L22607, doi:10.1029/2010GL045272 (2010).
[10]C. P. Caulfield and W. R. Peltier, "Anatomy of the mixing transition in homogeneous and stratified free shear layers," J. Fluid Mech. **413**, 1 (2000).
[11]J. R. Taylor, "Numerical simulations of the stratified oceanic bottom layer," Ph.D. thesis (University of California, San Diego, 2007).
[12]E. N. Lorenz, "Available potential energy and the maintenance of the general circulation," Tellus **7**, 157 (1955).
[13]K. Winters, P. Lombard, J. Riley, and E. A. D'Asaro, "Available potential energy and mixing in density-stratified fluids," J. Fluid Mech. **289**, 115 (1995).
[14]T. R. Osborn, "Estimates of the local rate of vertical diffusion from dissipation measurements," J. Phys. Oceanogr. **109**, 83 (1980).
[15]W. D. Smyth, J. N. Moum, and D. R. Caldwell, "The efficiency of mixing in turbulent patches: Inferences from direct simulations and microstructure observations," J. Phys. Oceanogr. **31**, 1969 (2001).
[16]W. R. Peltier and C. P. Caulfield, "Mixing efficiency in stratified shear flows," Annu. Rev. Fluid Mech. **35**, 135 (2003).